X-ray Diffraction and Theoretical Calculation–Supported Formation of Polymorphic Cocrystals Discovered Through Thermal Methods: A Case Study

Zhengzheng Zhou, Monica Calatayud, Julia Contreras-García, Liang Li, Henry H y Tong, Ying Zheng

Accepted Manuscript

X-ray Diffraction and Theoretical Calculation-Supported Formation of Polymorphic Cocrystals Discovered through Thermal Methods: A Case Study

Zhengzheng Zhou, Mónica Calatayud, Julia Contreras-García, Liang Li, Henry H.Y. Tong, Ying Zheng

PII: S0022-3549(19)30321-1

DOI: https://doi.org/10.1016/j.xphs.2019.05.019

Reference: XPHS 1600

To appear in: *Journal of Pharmaceutical Sciences*

Received Date: 16 February 2019

Revised Date: 24 April 2019

Accepted Date: 14 May 2019

Please cite this article as: Zhou Z, Calatayud M, Contreras-García J, Li L, Tong HHY, Zheng Y, X-ray Diffraction and Theoretical Calculation-Supported Formation of Polymorphic Cocrystals Discovered through Thermal Methods: A Case Study, *Journal of Pharmaceutical Sciences* (2019), doi: https://doi.org/10.1016/j.xphs.2019.05.019.

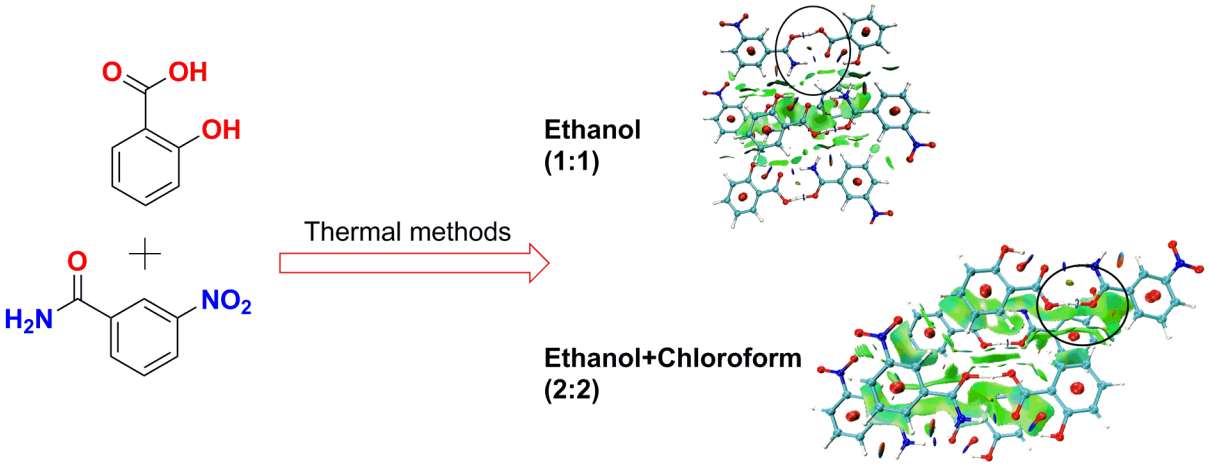

X-ray Diffraction and Theoretical Calculation-Supported Formation of Polymorphic Cocrystals Discovered through Thermal Methods: A Case Study

Zhengzheng Zhou,[a] *Mónica Calatayud,*[*b] *Julia Contreras-García,*[b] *Liang Li,*[c] *Henry H. Y., Tong,*[d] *Ying Zheng,*[*e]

[a] Department of Hygiene Inspection & Quarantine Science, Guangdong Provincial Key Laboratory of Tropical Disease Research, School of Public Health, Southern Medical University, Guangzhou, Guangdong 510515, China

[b] Sorbonne Universités, Laboratoire de Chimie Théorique, UPMC Univ Paris 06, CNRS, CC 137-4, place Jussieu F., 75252 Paris Cedex 05, France

[c] Department of Forensic Toxicological Analysis, Zhongshan School of Medicine, Sun Yat-Sen University, Guangzhou, 510080, China

[d] School of Health Sciences, Macao Polytechnic Institute, Macao SAR, China

[e] State Key Laboratory of Quality Research in Chinese Medicine, Institute of Chinese Medical Sciences, University of Macau, Macao SAR, China

[*]To whom correspondence should be addressed:

Ying Zheng, Ph.D.

E-mail: yzheng@umac.mo

Monica Calatayud, Ph. D.

E-mail: calatayu@lct.jussieu.fr

ABSTRACT

Polymorphism commonly exists in the preparation of cocrystals and has attracted widespread attention from both the pharmaceutical industry and academia. However, few studies have examined how to discover polymorphic cocrystals and their potential formation mechanism. In this study, we report the novel discovery of salicylic acid: 3-nitrobenzamide (SA-3NBZ) polymorphic cocrystals by thermal methods. The formation mechanism is elucidated based on theoretical calculations. SA-3NBZ polymorphic cocrystals with molar ratio of 1:1 and 2:2 were discovered using the combination of differential scanning calorimetry (DSC) and hot stage microscopy (HSM). Single crystal X-ray diffraction analysis confirmed this discovery. Density functional theory (DFT) calculations corrected with dispersion were conducted to illustrate the energetic stabilization of SA polymorphic cocrystals. Compared with the starting materials, formation of the cocrystals at 1:1 and 2:2 present a weak stabilization with overall energy reduction of -0.01 and -0.05 eV/molecule, respectively. The calculated non-covalent interactions index (NCI) further suggests that intralayer hydrogen bonds and van der Waals forces contribute to these weak interactions. The DFT calculations are in good agreement with the X-ray diffraction data. Hence, thermal analysis is a simple and reliable method to discover polymorphic cocrystals.

Key words

Salicylic acid, cocrystal, polymorphism, density functional theory (DFT), thermal methods, modulated temperature DSC (MTDSC)

INTRODUCTION

Cocrystals are crystalline single-phase materials composed of two or more different molecules with certain stoichiometric ratios based on non-covalent/ionic interactions under ambient conditions.[1,2] Cocrystallization is increasingly attractive to pharmaceutical scientists because it allows for the design of new solid-states to regulate the physicochemical properties of active pharmaceutical ingredients (APIs), eventually leading to the discovery of promising drug candidates.[3-5] Polymorphic or stoichiometric cocrystals may appear between the same API and cocrystal former (CCF).[6, 7] Polymorphic/stoichiometric cocrystal discovery is a rapidly growing and interesting aspect of crystal growth because physiochemical properties change, including solubility,[8, 9] dissolution,[10] permeability/ diffusion[11] and even stability[12, 13] corresponding to each cocrystal. Since cocrystals with polymorphic or stoichiometric diversity are a significant point in the development of pharmaceutical formulations, how to approach this in cocrystal formation remains an unanswered question. So far, several methods have been developed to observe these particular cocrystals. Process analytical technologies (PAT)-based design of agrochemical cocrystal was established to observe this phenomenon.[14] Grinding conditions and starting materials are potential significant points in the formation of cocrystals with polymorphic or stiochiometric diversity.[15-17] However, few studies have been performed to discover polymorphic cocrystals using thermal methods. Heat-induced cocrystallization has attracted increasing attention because it is an alternative green and reliable method that does not utilize organic solvents in comparison to other methods.

In our previous study, a reliable and simple thermal method consisting of differential scanning calorimetry (DSC) and hot stage microscopy (HSM) was developed to discover stoichiometric cocrystal systems.[18] The thermal behavior of API and CCF physical mixtures can be used to determine whether it is capable of cocrystal formation. Stoichiometric cocrystal formation presents unique thermodynamic action, showing three endotherms and two exotherms. When a physical mixture of API and CCF is heated using DSC, two exothermic peaks should be detected. Exothermic behavior on the DSC profile corresponds a new phase generation.[19-21] The Kofler mixed fusion method conducted by HSM can be used to confirm the DSC results.[22] The new cocrystal can be determined

when a new phase strip zone is generated. It should be noted that a polymorphic cocrystal is a special form that differs from a stoichiometric cocrystal.

In the present study, we aimed to discover new polymorphic cocrystals by thermal methods and elucidate the structural stability and mechanism using theoretical calculations. Salicylic acid (SA), an interesting phenolic compound, was selected as model drug. It is used as a topically keratolytic agent, and so far, there are over thirty cocrystals and various types of salts that have been reported.[23] The crystal nucleation study of SA has demonstrated that nucleation properties change in different solvents.[24] SA exists predominately as dimers in chloroform with no clear evidence of dimerization in other investigated solvents. The combination thermal methods of DSC and HSM were used to discover potential SA polymorphic cocrystals. Two new polymorphic cocrystals (1:1, 2:2) between SA and 3-nitrobenzamide (3NBZ) were obtained and identified using X-ray diffraction. The total energy for the starting materials and two new cocrystals were calculated. Intralayer hydrogen bonds and van der Waals forces hold up the weak interactions of cocrystals through non-covalent interactions index (NCI) analysis. All theoretical calculations are in good agreement with experimental data.

MATERIALS AND METHODS

Materials

SA and 3NBZ (HPLC purity > 98.0%) were purchased from J & K Chemical, Ltd. (Beijing, China) and Sigma Aldrich (Missouri, USA) respectively. Organic solvents were purchased from Guangzhou Chemical Factory (Guangzhou, China). All chemicals were of analytical grade and used without further purification. Distilled water was obtained from a Millipore ultra-pure water system in our lab (Bedford, USA). The molecular structures are presented in Scheme. 1.

Polymorphic Cocrystal Preparation

SA-3NBZ (1:1): Cocrystallization can be conducted by two methods: liquid assisted grinding (LAG) and the slow evaporation solution method (SESM). **LAG:** A mixture of SA (15.8 mg) and 3NBZ (16.6 mg) with a 1:1 molar ratio were weighed, mixed with drops of ethanol, then the mixture was ground for 30 s in an agate mortar. The solids were collected and dried at 40 °C for one hour. **SESM:** A mixture of SA (15.8 mg) and 3NBZ (16.6 mg) were dissolved in an ethanol solution, heating to 50 °C for 30 min. Then, the solution was filtered by a 0.45 μm filtrate

membrane in a vial. The vial was sealed with parafilm with several holes. The single crystals were obtained after three days.

SA-3NBZ (2:2): The cocrystal was obtained by the SESM method. A mixture of SA (15.8 mg) and 3NBZ (16.6 mg) were dissolved in a mixed ethanol: chloroform solution (1:1, v/v) and heated to 50 °C for 30 min. The solution was filtered with a 0.45 μm filtrate membrane and transferred into another vial. The vial was sealed, poking several holes on the surface. The crystals and solids were harvested after three days.

Solid State Characterization

DSC analyses were performed on a Shimadzu DSC-60A instrument (Tokyo, Japan). The scans over the range of 50 °C to 200 °C were performed with the heating rates of 2, 5, 10, and 20 °C.min^{-1}. All DSC analytes were run under a continuous nitrogen atmosphere with a stable flow rate (35 mL.min^{-1}).

Modulated temperature DSC (MTDSC) analyses were performed at a step scan criteria within 0.01 °C on a PerkinElmer DSC 8000 instrument (Waltham, USA). The temperature program was set as follows: first, holding for 1.0 min at 75 °C, then stepping scan with a heating rate of 5 °C.min^{-1}, going to the next isothermal repetition (1 min) if the subtracted heat flow equilibrates within +/- 0.0100, finally holding for 2.0 min at 155 °C. Both DSC instruments were calibrated with indium certified reference material (222-10950-91, purity 99.999%, Japan).

An Olympus BX53 polarizing microscope (Tokyo, Japan) coupled with a Linkam THMS600 hot stage (London, UK) was used to perform HSM experiments. The detailed procedure was set as follows: first, the higher melting temperature component was heated to melt and then solidify on the glass slide; second, another lower melting temperature component was heated to melt, placing it in touch with the previous material then cooling to room temperature.

Single crystal X-ray diffraction data were obtained with an Agilent Technologies Gemini A Ultra system using graphite monochromated Cu *Kα* radiation (λ= 1.5418 Å). All structures were solved by the Olex 2 program and refined by the full-matrix least-squares method on F^2 using SHELXS 97.[25, 26]

Powder X-ray diffraction (PXRD) patterns were collected using a Philips PW1830 X-ray powder diffraction system (Almelo, Netherlands). The 2θ range was set from 5.0º to 40.0º with a 0.05º step size on Cu *Kα* (λ= 1.5418 Å) mode.

Theoretical Calculations

Based on the experimental synthesis of the cocrystals formed between SA and 3NBZ, a computational study was conducted to characterize the stability of the mixed materials. Three steps were performed: (1) a geometric energetic study, in which the structures were optimized and compared to the experimental crystallographic data; (2) an energetic study to assess the stability of the cocrystals; and (3) bonding analysis in which the intermolecular interactions were analyzed based on the noncovalent index. Periodic density functional theory (DFT) calculations were performed using the VASP code 5.4.1 with the PBE function.[27-31] Dispersion interactions are included by the Grimme D3 approach[32] as implemented in the code. Valence electrons are explicitly treated with the basis set of 520 eV, and core electrons are replaced by plane augmented wave pseudopotentials.[33, 34] The Brillouin zone is sampled with k-points at the spacing of 0.02 $Å^{-1}$. The threshold for an electronic iteration is 0.1 meV and is 1 meV for an ionic iteration. Geometry optimization was performed with the conjugate-gradient algorithm with all atoms and unit cell shapes and dimensions allowed to relax. The initial geometry was taken from the following references: SA monoclinic,[34, 35] 3NBZ monoclinic,[36] 1:1 and 2:2 cocrystals (from this work). The interaction energy E_{int} is calculated as the difference between the energies of the cocrystals (composition of *N* (SA): *N* (3NBZ) and the pure crystals and is given per molecule (eq 1),

$$E_{\text{int}} = (E_{crystal}[SA_N\,3NBZ_N] - NE_{SApure} - NE_{3NBZpure})/N \qquad \text{eq (1);}$$

No zero-point energy correction is considered at this time. The analysis of the noncovalent interactions was performed by means of the NCI. On the basis of electron density and its derivatives (eq 2), the index maps the noncovalent interactions through a reduced gradient (s (ρ)).

$$s(\rho) = \frac{|\nabla\rho|}{c_F\rho^{4/3}} \qquad \text{eq (2);}$$

NCI isosurfaces enable visualization of the molecular interactions in the same system. Attractive and repulsive contributions could be separated based on the second eigenvalue (λ_2) sign of the electron-density, Hessian matrix at each point: usually repulsion appears at positive values of λ_2, hydrogen bonds appear at negative values, and dispersion appears at values close to zero. All interactions could be distinguished to color the isosurfaces based on these principles

(sign (λ_2) ρ). The color code was defined as follows: the covalent bonds and highly attractive weak interactions (such as hydrogen bonds) are in blue, extremely weak interactions (such as very weak H-H interactions and van der Waals interactions) are in green, and repulsive interactions (e.g., steric repulsions) are in red.

RESULTS

Polymorphic Cocrystal Discovery by Thermal Methods

Thermal methods consisting of DSC and HSM are reliable and simple for stoichiometric cocrystal discovery. The thermal behavior of cocrystals with stoichiometric diversity presents significant characteristics. Figure 1 (left) presents the DSC profiles of SA-3NBZ physical mixtures (1:1, molar ratio) with different heating rates varying from 2 °C.min^{-1} to 20 °C.min^{-1}. Apart from the endotherms and exotherms observed in all profiles, the lower heating rate (2 °C.min^{-1}) displays better thermal resolution, which could manifest slight variations. Interestingly, the thermal behavior at 2 °C.min^{-1} corresponds to the cocrystals with stoichiometric diversity. The results demonstrate three endotherms at T_{onset} = 109.1, 115.2 °C and 86.1 °C, as well as two exotherms. The thermal analysis results indicate that the SA-3NBZ system may form stoichiometric cocrystals. Reversing and nonreversing MTDSC are conducted to investigate the complex phase transition.[37, 38] Figure 1 (right) presents the MTDSC results. The reversing heat flow curve demonstrates the heat capacity-related stable crystalline phase, while the nonreversing heat flow curve shows the meta-stable thermodynamic crystalline phase. Observing several endotherms and exotherms in reversing mode can clearly indicate the new phase generation experiences that complicate the recrystallization process. In the nonreversing mode curve, two separate endotherms can be observed clearly that differs from the reversing mode curve. The MTDSC results confirm the potential stoichiometric cocrystal formation.

Then, HSM observations were performed to confirm the DSC results. The mixing zone of SA and 3NBZ present the new cocrystal phase at 113 °C, followed by a strip forming at 117 °C, which finally disappears at 118 °C (Fig. 2.). The endothermic temperatures of the new phase and the strip formation slide in comparison with DSC results due to the heating conduction time delays. Only one strip can be observed, even though the heating rate is set as 1 °C.min^{-1}. This indicates that a new cocrystal was generated in the SA-3NBZ system. However, there is no stoichiometric diversity zone in the HSM profiles.

This is inconsistent with the DSC results. It is speculated that cocrystals with special forms may be generated, especially unstable or meta-stable polymorphic cocrystal. Two heating cycles under HSM result in the potential rapid transformation to the most stable solid form.

Figure 3 presents the DSC profiles of cocrystals obtained with a heating rate at 10 °C.min^{-1}. The SA-3NBZ (1:1) cocrystal presents one sharp endotherm with an onset temperature of 114.5 °C. The SA-3NBZ (2:2) cocrystal presents two endotherms (110.3 °C, 115.6 °C) in the DSC profile. It is speculated that the melting point of the SA-3NBZ (2:2) cocrystal is 110.3 °C, while the mixed (1:1) cocrystal exhibits its endotherm at 115.6 °C. The onset temperatures of both 1:1 and 2:2 cocrystals shift approximately 1 °C because the peak integration location changed. However, the chemical pure SA-3NBZ (2:2) cocrystal cannot be obtained using many methods despite the boosted dimer nucleation in chloroform.

X-ray Diffraction Characterization

Table 1 presents all the crystallographic data. SA-3NBZ (1:1) belongs to the monoclinic $P2_1$ space group with a = 6.335 **Å**, b = 30.573 **Å**, c = 7.404 **Å**, β = 106.004°, V = 1378.54 **Å^3**. The SA molecule links to the 3NBZ molecule through N_2-H$\cdots$$O_2$ and O_3-H$\cdots$$O_4$ intermolecular hydrogen bonds to form a ring; it also forms another ring through the O_1-H$\cdots$$O_2$ intramolecular hydrogen bond, leading to a 1D wave strip (Fig. 4a). The adjacent 1D chains are further connected via N_2-H$\cdots$$O_1$ hydrogen bonds to generate a 2D sheet (Fig. 4b). A 3D structure is formed by the adjacent 2D sheets based on van der Waals forces (> 5 Å, Fig. 4c). SA-3NBZ (2:2) crystallizes in a monoclinic *I*a structure with unit cell dimensions of a = 21.784 **Å**, b = 5.172 **Å**, c = 25.340 **Å**, β = 104.792°, V = 2760.3 **Å^3**. Each SA molecule is linked to a 3NBZ molecule through two types: the first joint type is through N_4-H$\cdots$$O_5$, N_2-H$\cdots$$O_4$, N_2-H$\cdots$$O_2$ intermolecular hydrogen bond and O_4-H$\cdots$$O_5$, O_1-H$\cdots$$O_2$ intramolecular hydrogen bond to form a 2D sheet; the second joint type is through N_4-H$\cdots$$O_1$, N_2-H$\cdots$$O_2$, N_2-H$\cdots$$O_4$ intermolecular hydrogen bond and O_4-H$\cdots$$O_5$, O_1-H$\cdots$$O_2$ intramolecular hydrogen bond to form another 2D structural unit (Fig. 5a) . A cross structure is formed owing to the two 2D sheets by van der Waals forces (Fig. 5b). The cross molecular arrangement in the crystal lattice is consistent with SA.[24] SA molecules are held together via van der Waals forces (plane distances > 5 Å).

Figure 6 presents the experimental and calculated PXRD patterns for SA-3NBZ cocrystals. The experimental PXRD pattern of the SA-3NBZ (1:1) cocrystal presents high similarity and

phase purity in comparison with the theoretical results. Characteristic peaks for the SA-3NBZ (1:1) cocrystal at 2θ: 5.7°, 15.0°, 17.1°, 18.5°, 18.9°, 26.2° and 27.4° can be observed on the PXRD patterns. However, the experimental PXRD pattern for the SA-3NBZ (2:2) cocrystal presents low phase purity. The characteristic peaks of the SA-3NBZ (1:1) experimental PXRD pattern can be observed at 9.9°, 21.2° and 22.6°, while mixing characteristic peaks (15.1°, 17.7° and 26.2°) of the SA-3NBZ (1:1) cocrystal can be obviously observed. These results are consistent with DSC data.

Theoretical Calculation

To gain further insight into the stability of SA-3NBZ (1:1, 2:2), a computational study based on DFT corrected for dispersive interactions was developed in the present study. The structures of the pure crystals and cocrystals were optimized with respect to cell shape and dimensions as well as ionic positions. Table 2 displays the experimental and optimized parameters obtained. It can be observed that for the four structures considered, the calculated parameters are in excellent agreement with the experimental data. Upon optimization, the structures stay monoclinic with deviations of less than one degree for the angle. The lattice vectors are slightly underestimated by less than 2% with respect to the experimental values, resulting in a weak shrinking of the unit cell volume of at most 2.2%. Note that the use of DFT was not corrected for dispersion results in a severe overestimation of the geometrical parameters (not shown).

The total energy per molecule including dispersion corrections for the calculated systems are displayed in Table 3. The contribution of the dispersion interaction is also shown and is found to be more important for the extended systems (pure and cocrystals) than for the gas-phase systems. The pure crystals are stabilized by -1.30 eV (SA) and -1.39 eV (3NBZ) with respect to the gas-phase molecules. The cocrystals are only weakly stabilized with respect to the pure crystals, -0.01 eV (1:1) and -0.05 eV (2:2). This may indicate the meta-stability of the cocrystals with respect to the pure phases. In the SA-3NBZ (2:2), 3NBZ is formed by dimers, where the O and the NH_2 groups face one another, leading to a symmetric local structure. Cocrystals show a very interesting structure where the two molecules are joined together by a resonant hydrogen bond. Interestingly, the OHO distances are extremely short. These suprastructures are arranged in a parallel manner in the perpendicular axis, with a benzene stacking on top of the resonant structure, leading to van der Waals interactions. This is highlighted in Figure 7

using the visualization of the NCI method.[39, 40] Hydrogen bonds appear as blue circles, and van der Waals interactions can be visualized as extended green surfaces within this approach. Figure S1a, c highlights the double hydrogen bond and the stacking of layers in the 1:1 cocrystal, respectively. Figure S1b, d present the 2:2 arrangements (see Fig. S1 for a schematic view of the arrangement). An important difference is also highlighted in Figure S1d: the appearance of hydrogen-bonded networks between the layers, contributing to the stability of the dimer cocrystal.

DISCUSSIONS

Polymorphic Cocrystal Discovery and Preparation

The stoichiometric/polymorphic cocrystals screening procedure for SA was performed using thermal methods. Three endotherms (representing a eutectic point and two melting points) and two exotherms (representing new recrystallization) can be observed clearly on the DSC diagrams of SA-3NBZ system. MTDSC presents a better way than common DSC to observe these complex thermal behaviors in the present study. The reversing and nonreversing curves clearly demonstrate the recrystallization procedures. HSM can be used as a helper method to confirm DSC discovery. However, SA-3NBZ cocrystals with stoichiometry cannot be prepared for a long time by many methods including LAG, SESM, rapid solvent removal and even the slurry method. Only SA-3NBZ (1:1) is prepared and repeated multiple times. It is speculated that the unprepared cocrystal maybe a meta-stable solid phase. The meta-stable property hinders us obtaining it from experiments. Notably, the crystal nucleation of SA changed in different solvents.[24] The SA dimer can be formed in chloroform solution, and chloroform was selected as a wetting organic solvent in LAG method based on a previous study. PXRD results have demonstrated slightly different peaks (Fig. S2.). Considering the nucleation can be correlated with chloroform, over fifty cocrystal preparation experiments at different concentrations using the slow evaporation method were designed and performed in this work. Finally, SA-3NBZ (1:1, 2:2) polymorphic cocrystals were obtained.

Solid Characterization and Theoretical Calculation

For the SA-3NBZ cocrystals, different intermolecular hydrogen bonds can be determined by X-ray diffraction analysis. Although the accurate molecular structures can be characterized by single X-ray diffraction analysis, the bulk sample with high phase purity

for SA-3NBZ (2: 2) cannot be prepared. SA-3NBZ (1: 1) always mixed together with SA-3NBZ (2:2) even in chloroform solution. Two sharp endotherms from SA-3NBZ (2:2) can be clearly observed in Figure 3. As the higher melting point is determined for the SA-3NBZ (1:1), 110.3 °C is easily assigned as the melting point for the SA-3NBZ (2:2). The DSC and PXRD results both indicate low phase purity for SA-3NBZ (2:2) and high phase purity for SA-3NBZ (1:1).

The unusual preparation method of SA-3NBZ (2:2) bulk sample with low phase purity may have two possible reasons. First, the organic solvent influences the cocrystallization of SA. Many other organic solvents such as ethanol, methanol and acetone are used in this work. No evidence supports the formation of SA-3NBZ polymorphic cocrystals. Second, interaction energy (-0.05 ev) of SA-3NBZ (2:2) indicates lower stability than 1:1 SA-3NBZ (-0.01 ev). The cocrystallization is inclined to form a more stable phase. The total energy of both cocrystals is calculated as -913.18 ev (1: 1) and -1826.68 ev (2: 2) respectively. The negative values indicate an exothermic reaction. Now, we extend the concept to why polymorphic cocrystals can be discovered by thermal methods. The reliable DSC records and energy calculation based on single crystal X-ray diffraction data present a reasonable explanation: (1) Two distinctive endotherms (114.5 °C and 110.3 °C) for both cocrystals guarantee this finding, and (2) a large energy barrier (>900 ev) between the polymorphic cocrystals prevents direct phase transformation.

CONCLUSIONS

In summary, the present study reports the discovery of two new polymorphic cocrystals composed of SA and 3NBZ (1:1 and 2:2, molar ratio) using thermal methods. Interestingly, a SA-3NBZ (2:2) was obtained and confirmed by X-ray diffraction analysis for the first time. Theoretical calculations corrected with dispersion indicate a weak energetic stabilization of the obtained cocrystals 1:1 (-0.01 eV/molecule) and 2:2 (-0.05 eV/molecule). The theoretical calculation based on X-ray diffraction supports distinctive endotherms with large energy barriers are in favor of gazing polymorphic cocrystals.

ACKNOWLEDGMENTS

We are grateful for financial support from the Research Committee of University of Macau (Ref. No. MYRG2016-00090-ICMS-QRCM) and Natural Science Foundation of China (81703438). MC is grateful for the HPC resources from GENCI- CINES/IDRIS

(Grant 2017- x2017082131, 2016- x2016082131) and the CCRE-DSI of Université P. M. Curie. This work was conducted within the frame of the H2020 ITN-Eurasiacat programme 552067-EM-1-2014-1-ES-ERA MUNDUS-EMA22.

REFERENCES

1. Xu J, Huang Y, Ruan S, Chi Z, Qin K, Cai B, Cai T. 2016. Cocrystals of isoliquiritigenin with enhanced pharmacokinetic performance. CrystEngComm 18: 8776-8786.
2. Luo Y, Chen S, Zhou J, Chen J, Tian L, Gao W, Zhang Y, Ma A, Li L, Zhou Z. 2019. Luteolin cocrystals: characterization, evaluation of solubility, oral bioavailability and theoretical calculation. J Drug Deliv Sci Tec 50: 248-254.
3. Zhou Z, Li W, Sun WJ, Lu T, Tong HHY, Sun CC, Zheng Y. 2016. Resveratrol cocrystals with enhanced solubility and tabletability. Int J Pharmaceut 509: 391-399.
4. Cao F, Rodriguez-Hornedo N, Amidon GE. 2019. Mechanistic analysis of cocrystal dissolution, surface pH, and dissolution advantage as a guide for rational selection. J Pharm Sci 108: 243-251.
5. Battini S, Mannava MKC, Nangia A. 2018. Improved stability of tuberculosis drug fixed-dose combination using isoniazid-caffeic acid and vanillic acid cocrystal. J Pharm Sci 107: 1667-1679.
6. Babu NJ, Reddy LS, Aitipamula S, Nangia A. 2008. Polymorphs and polymorphic cocrystals of temozolomide. Chem Asian J 3: 1122-1133.
7. Fu Q, Han Y, Xie Y, Gong N, Guo F. 2018. Carbamazepine cocrystals with several aromatic carboxylic acids in different stoichiometries: Structures and solid state characterization. J Mol Struct 1168: 145-152.
8. Lipert MP, Rodriguez-Hornedo N. 2015. Cocrystal transition points: role of cocrystal solubility, drug solubility, and solubilizing agents. Mol Pharmaceutics 12: 3535-3546.
9. Sokai A, Pindelska E, Szeleszczuk L, Kolodziejski W. 2017. Pharmaceutical properties of two ethenzamide-gentisic acid cocrystal polymorphs: drug release profiles, spectroscopic studies and theoretical calculations. Int J Pharmaceut 522: 80-89.
10. Li Z, Matzger AJ. 2016. Influence of coformer stoichiometric ratio on pharmaceutical cocrystal dissolution: three cocrystals of carbamazepine/4-aminobenzoic acid. Mol Pharmaceutics 13: 990-995.
11. Saikia B, Bora P, Khatioda R, Sarma B. 2015. Hydrogen bond synthons in the interplay of

solubility and membrane permeability/diffusion in variable stoichiometry drug cocrystals. Cryst Growth Des 15: 5593-5603.

12. Grossjohann C, Serranon DR, Paluch KJ, O'Connell P, Vella-Zarb L, Manesiotis P, McCabe T, Tajber L, Corrigan OI, Healy AM. 2015. Polymorphism in sulfadimidine/4-aminosalicylic acid cocrystals: solid-state characterization and physicochemical properties. J Pharm Sci 104: 1385-1398.
13. Orola L, Veidis MV. 2009. Nicotinamide fumaric acid supramolecular cocrystals: diversity of stoichiometry. CrystEngComm 11: 415-417.
14. Powell KA, Croker DM, Rielly CD, Nagy ZK. 2016. PAT-based design of agrochemical co-crystallization process: A case-study for the selective crystallization of 1:1 and 3:2 co-crystals of p-toluenesulfonamide/triphenylphosphine oxide. Chem Eng Sci 152: 95-108.
15. Trask AV, Streek J, Samuel Motherwell WD, Jones W. 2005. Achieving polymorphic and stoichiometric diversity in cocrystal formation: importance of solid-state grinding, powder X-ray structure determination, and seeding. Cryst Growth Des 5: 2233-2241.
16. Limwikrant M, Nagai A, Hagiwara Y, Higashi K, Yamamoto K, Moribe K. 2012. Formation mechanism of a new carbamazepine/malonic acid cocrystal polymorph. Int J Pharmaceut 431: 237-240.
17. Yuan Y, Wang L, Li D, Deng Z, Zhang H. 2018. How many parameters can affect the solid form of cocrystallization products in mechanochemical reactions? A case study. Cryst Growth Des 18: 7244-7247.
18. Zhou Z, Chan HM, Sung HHY, Tong HHY, Zheng Y. 2016. Identification of new cocrystal systems with stoichiometric diversity of salicylic acid using thermal methods. Pharm Res 33: 1030-1039.
19. Yamashita H, Hirakura Y, Yuda M, Teramura T, Terada K. 2013. Detection of cocrystal formation based on binary phase diagrams using thermal analysis. Pharm Res 30: 70-80.
20. Pal S, Roopa BN, Abu K, Manjunath SG, Nambiar S. 2014. Thermal studies of furosemide-caffeine binary system that forms a cocrystal. J Therm Anal Calorim 115: 2261-2268.
21. Lu E, Rodriguez-Hornedo N, Suryanarayanan R. 2008. A rapid thermal method for cocrystal screening. CrystEngComm 10: 665-668.
22. Berry DJ, Seaton CC, Clegg W, Harrington RW, Coles SJ, Horton PN, Hursthouse MB, Storey R, Jones W, Friščić T, Blagden N. 2008. Applying hot-stage microscopy to co-crystal

screening: a study of nicotinamide with seven active pharmaceutical ingredients. Cryst Growth Des 8: 1697-1712.

23. Sathisaran I, Dalvi SV. 2017. Crystal engineering of curcumin with salicylic acid and hydroxyquinol as coformers. Cryst Growth Des 17: 3974-3988.
24. Khamar D, Zeglinski J, Mealey D, Rasmuson ÅC. 2014. Investigating the role of solvent-solute interaction in crystal nucleation of salicylic acid from organic solvents. J Am Chem Soc 136: 11664-11673.
25. Dolomanov OV, Bourhis LJ, Gildea RJ, Howard JAK, Puschmann H. 2009. OLEX2: a complete structure solution, refinement and analysis program. J Appl Crystallogr 42: 339–341.
26. Sheldrick GM. 2008. A short history of SHELX. Acta Crystallogr A64: 112–122.
27. Kresse G, Hafner J. 1993. Ab initio molecular dynamics for open-shell transition metals. Phys Rev B 48: 13115-13118.
28. Kresse G, Hafner J. 1994. Norm-conserving and ultra soft pseudopotentials for first-row and transition elements. J Phys-Condens Mat 6: 8245.
29. Perdew JP, Burke K, Ernzerhof M. 1996. Generalized gradient approximation made simple. Phys Rev Lett 77: 3865-3868.
30. Perdew JP, Burke K, Ernzerhof M. 1997. Generalized gradient approximation made simple. Phys Rev Lett 78: 1396.
31. Grimme S, Antony J, Ehrlich S, Krieg H. 2010. A consistent and accurate Ab initio parametrization of density functional dispersion correction (Dft-D) for the 94 elements H-Pu. J Chem Phys 132: 154104.
32. Blochl PE. 1994. Projector augmented-wave method. Phys Rev B 50: 17953-17979.
33. Kresse G, Joubert D. 1999. From ultrasoft pseudopotentials to the projector augmented-wave method. Phys Rev B 59: 1758-1775.
34. Sundaralingam M. Jensen LH. 1965. Refinement of the structure of salicylic acid. Acta Crystallographica 18: 1053-1058.
35. Jia L, Svärd M, Rasmuson AC. 2017. Crystal growth of salycilic acid in organic solvents. Cryst Growth Des 17: 2964-2974.
36. Mem NK. 1987. Osaka Kyoiku Univ.Ser. 3: 36.

37. Gill PS, Sauerbrunn SR, Raading M. 1993. Modulated differential scanning calorimetry. J Therm Anal. 40: 931-939.
38. Prudic A, Ji Y, Sadowski G. 2014. Thermodynamic phase behavior of API/Polymer solid dispersions. Mol Pharmaceut. 11: 2294-2304.
39. Johnson ER, Keinan S, Mori-Sanchez P, Contreras-Garcia J, Cohen AJ, Yang W. 2010. Revealing noncovalent interactions. J Am Chem Soc 132: 6498-6506.
40. Contreras-Garcia J, Johnson E, Keinan S, Chaudret R, Piquemal JP, Beratan D, Yang W. J. 2011. NCIPLOT: a program for plotting non-covalent interaction regions. Chem Theor Comp **7**: 625-632.

Table 1. Crystallographic data of SA-3NBZ cocrystals

	SA-3NBZ (1:1)	**SA-3NBZ (2:2)**
Formula	$(C_7H_6O_3)$•$(C_7H_6N_2O_3)$	$(C_7H_6O_3)_2$•$(C_7H_6N_2O_3)_2$
formula weight	304.26	608.52
T (K)	173.00 (14)	150.00 (10)
crystal size (mm^3)	0.20×0.18×0.04	0.37×0.32×0.22
crystal system	Monoclinic	Monoclinic
space group	$P2_1/c$	*I*a
a (Å)	6.3351(3)	21.7838(11)
b(Å)	30.5729(10)	5.1719(3)
c (Å)	7.4045(3)	25.3404(19)
α (°)	90.00	90.00
β (°)	106.004(4)	104.792(7)
γ (°)	90.00	90.00
V($Å^3$)	1378.54(10)	2760.3(3)
Z	4	8
Z'	1	2
$\rho_{(calcd)}$ ($mg.m^{-3}$)	1.466	1.464
radiation type	Cu *Kα*	Cu *Kα*
*θ*range (°)	6.21-71.36	3.5850-66.4410
R_1 [$I>2\sigma(I)$]	0.0379	0.0467
Wr_2 (all data)	0.0955	0.1201
goodness-of-fit (on F^2)	1.006	1.065
CCDC	1060736	1404397

Table 2. Geometric parameters for the crystals considered: dimensions in Å, volume V in Å^3

	Pure crystals				**Cocrystals**			
	SA		**3NBZ**		**1:1**		**2:2**	
	Calc.[a]	Exp.[34, 35]	Calc.[a]	Exp.[36]	Calc.[a]	Exp.[a]	Calc.[a]	Exp.[a]
Z	8	8	4	4	4:4	4:4	8:8	8:8
a	11.394	11.52	12.739	12.776	6.288	6.3351	21.608	21.7838
b	11.224	11.21	7.797	7.809	30.618	30.5729	5.151	5.1719
c	4.843	4.92	7.690	7.842	7.283	7.4045	25.282	25.3404
a	90.000	90	90.000	90	90.000	90	90.000	90
b	91.859	90.83	106.697	106.94	105.622	106.004	104.833	104.792
c	90.000	90	90.000	90	90.000	90	90.000	90
V	618.99	635.3	731.630	748.43	1350.370	1378.54	2720.000	2760.33

[a] this work.

Table 3. Total E_T, dispersion E_{disp} and interaction E_{int} energy for the system calculated, in eV. The interaction energy is calculated with the formula given in the text, it is given per molecule, negative values indicate exothermic reaction

	E_T	E_{disp}	E_{int}
Gas-phase SA	-105.86	-0.18	
Gas-phase 3NBZ	-119.73	-0.22	
Pure crystal SA	-428.65	-3.86	-1.30[a]
Pure crystal 3NBZ	-484.49	-4.35	-1.39[a]
Cocrystal 1:1	-913.18	-8.25	-0.01[b]
Cocrystal 2:2	-1826.68	-16.20	-0.05[b]

[a] The gas-phase molecules SA and 3NBZ are considered for the evaluation of the pure phase stability.

[b] The pure crystals are considered for the calculation of the cocrystal stability.

Scheme. 1. Chemical structures of SA and 3NBZ

Figure Captions

Fig. 1. DSC (left) and MTDSC (right) results of SA-3NBZ physical mixture (1:1, molar ratio)

Fig. 2. The SA-3NBZ cocrystal generation zone observed by HSM (A= SA, B= 3NBZ, C= cocrystal)

Fig. 3. The DSC profiles of SA-3NBZ cocrystals with heating rate at 10 °C.min^{-1} (SA, black; 3NBZ, red; 1:1 cocrystal, blue; 2:2 cocrystal, green)

Fig. 4. (a) 1D chain, (b) side view (down) of 2D sheet and (c) 3D structure of SA-3NBZ (1:1)

Fig. 5. (a) 2D structural sheet, (b) 3D structure of SA-3NBZ (2:2)

Fig. 6. The experimental and calculated PXRD patterns for SA-3NBZ cocrystals (a, experimental for 1:1 cocrystal; a', calculated for 1:1 cocrystal; b, experimental for 2:2 cocrystal; b', calculated for 2:2 cocrystal;)

Fig. 7. Interaction network revealed by NCI: a) hydrogen bonding network in the 1:1 cocrystal; b) hydrogen bonding network in the 2:2 cocrystal; c) Packing interactions in the 1:1 cocrystal (van der Waals interactions (square) are highlighted); d) Packing interactions in the 2:2 cocrystal (the interface hydrogen bonded network is highlighted with a circle)

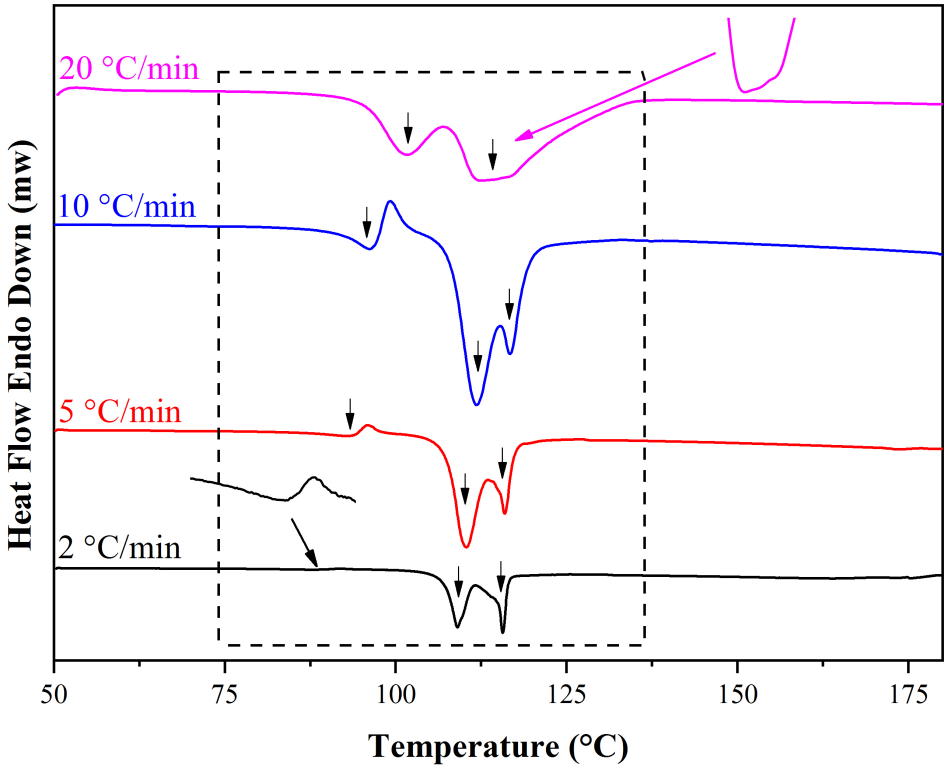

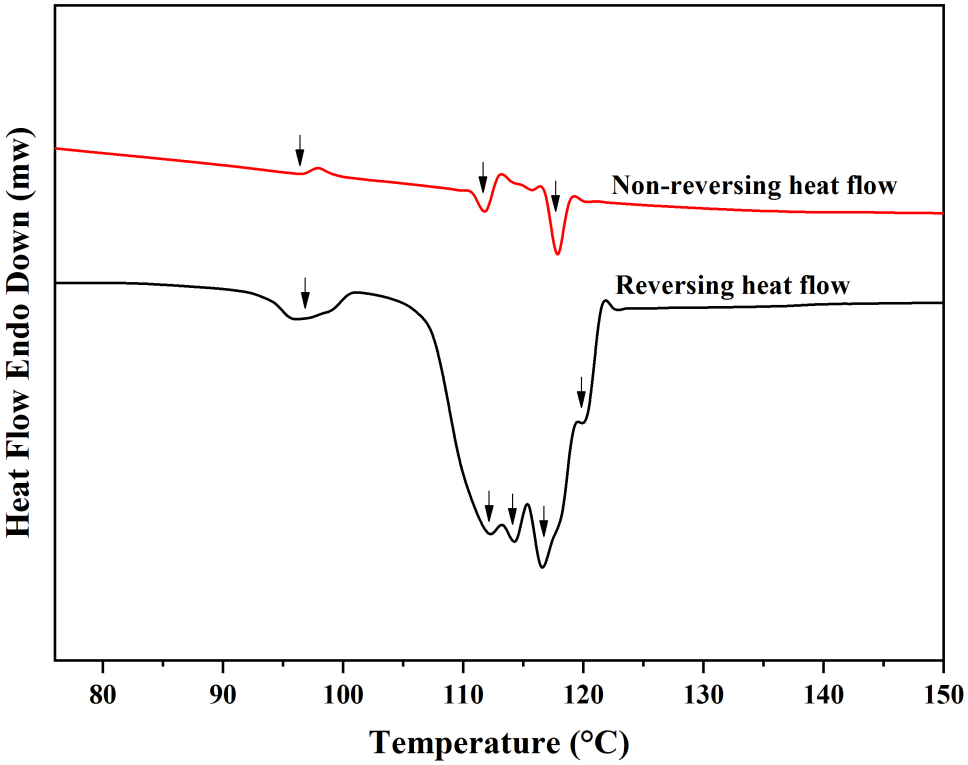

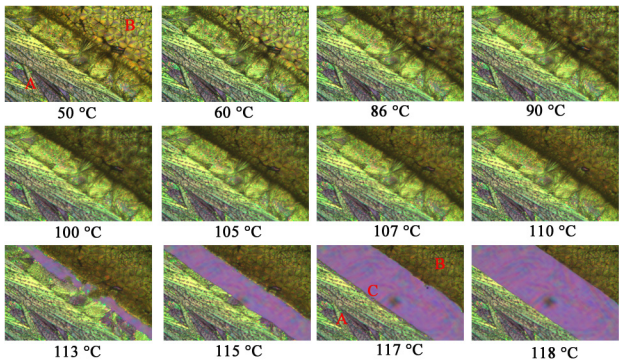

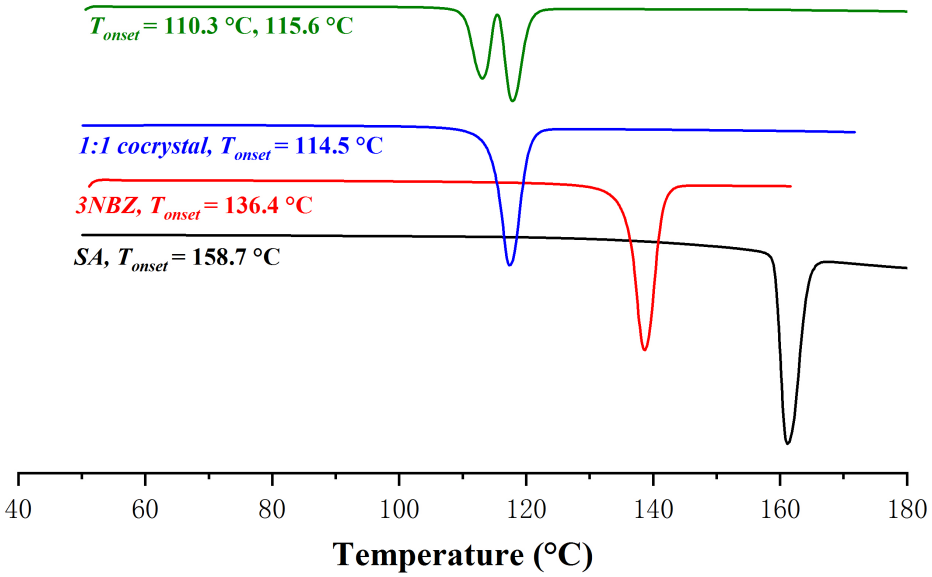

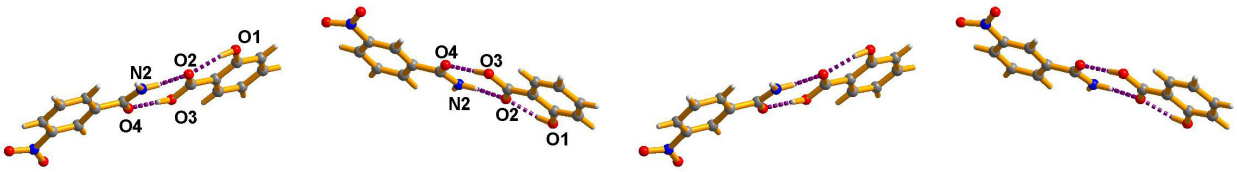

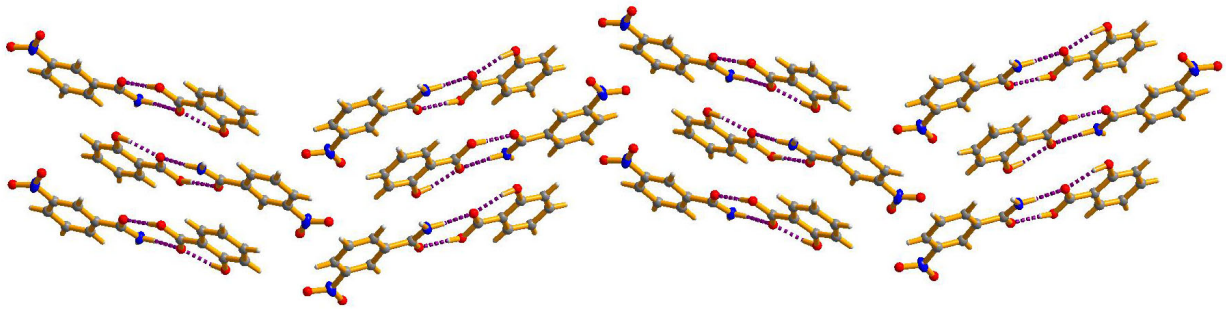

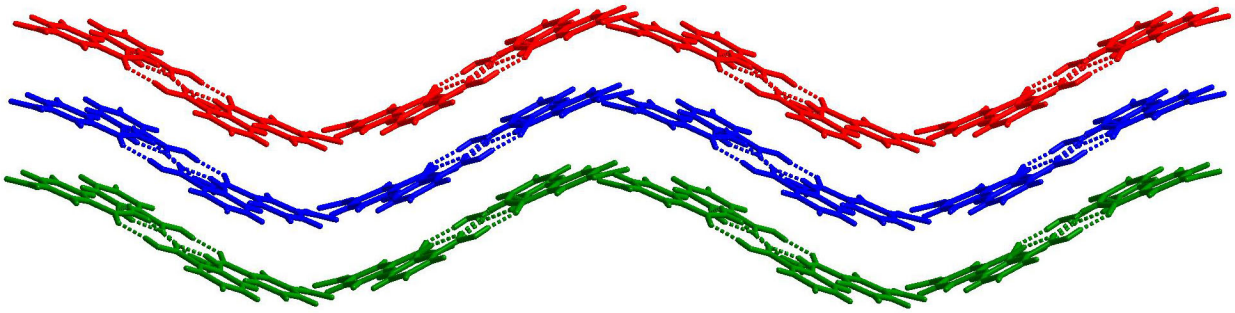

a

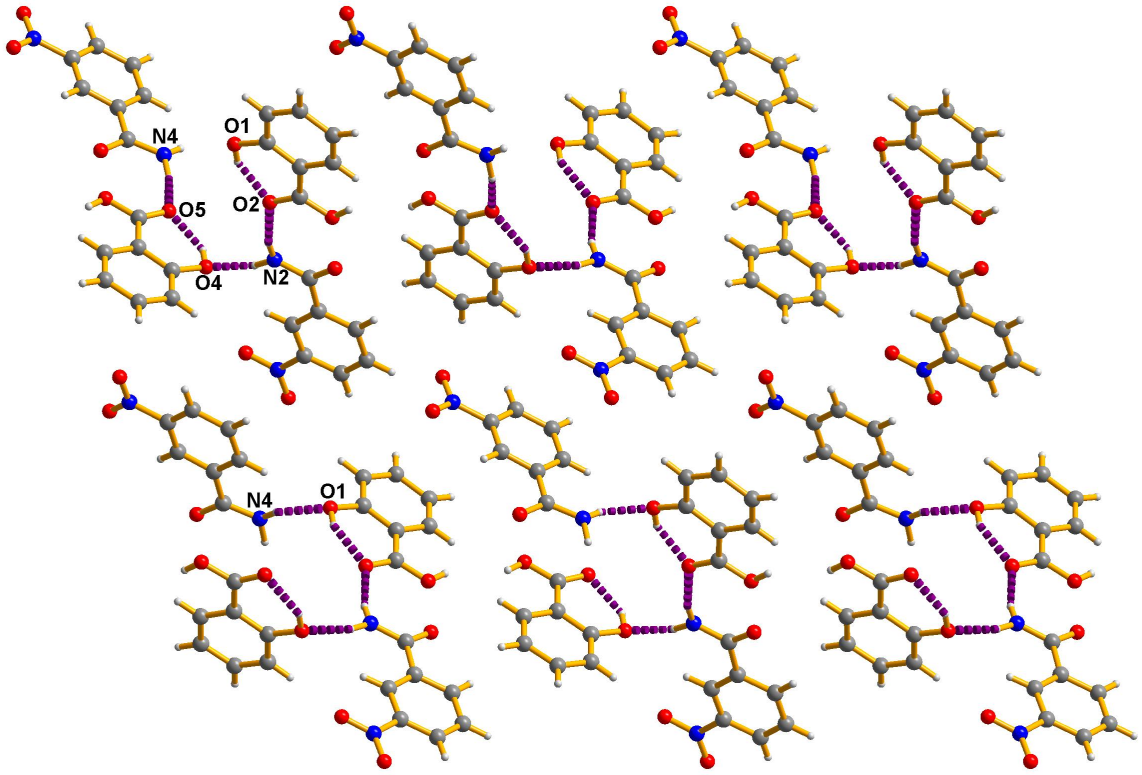

a

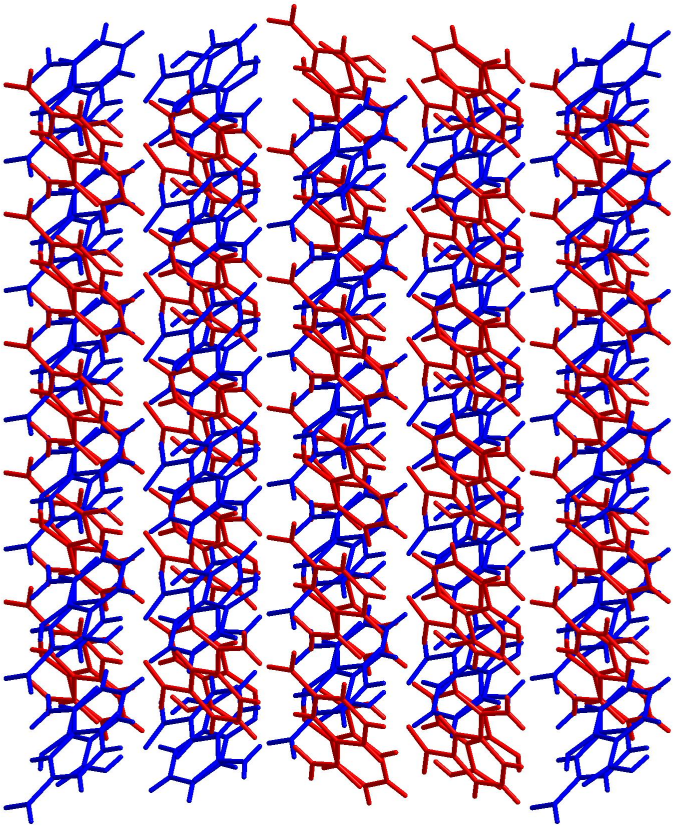

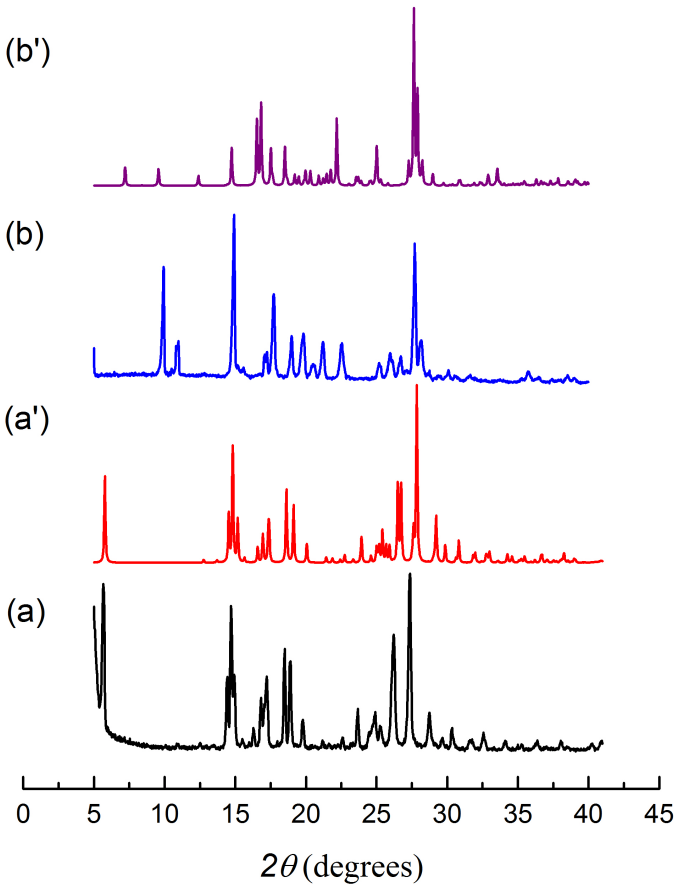

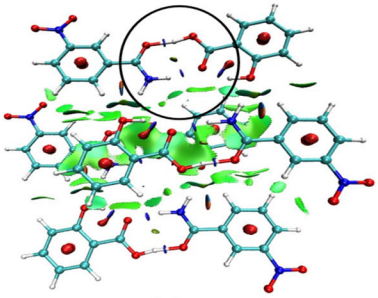

(a)

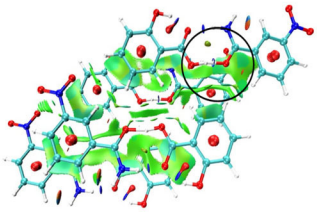

(b)

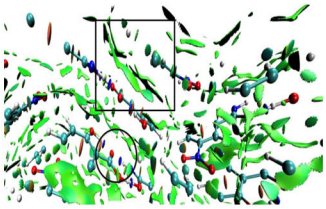

(c)

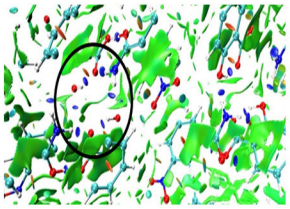

(d)

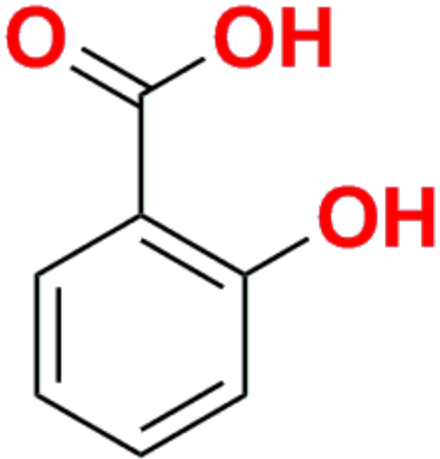

Salicylic acid, SA

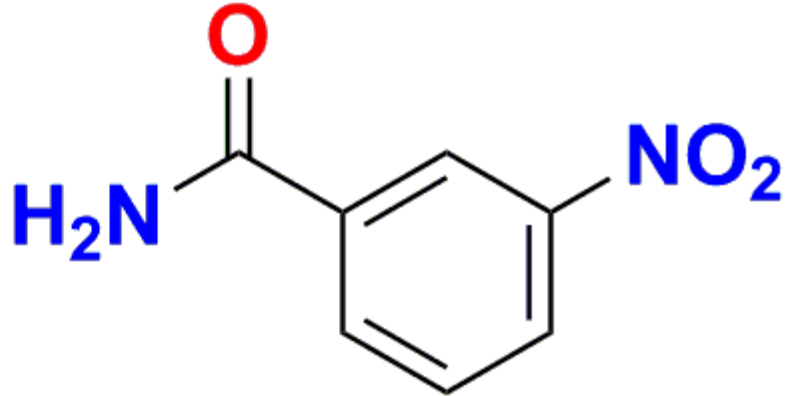

3-Nitrobenzamide, 3NBZ